World Journal of Microbiology and Biotechnology (2023) 39:281
https://doi.org/10.1007/s11274-023-03712-2

RESEARCH

Bacterial cell permeability study by metal oxide and mixed metal oxide nanoparticles: analysis of the factors contributing to the antibacterial activity of nanoparticles

Debashri Paul[1] · Ankur Pandey[2] · Sudarsan Neogi[1]

Received: 24 April 2023 / Accepted: 21 July 2023 / Published online: 17 August 2023

Abstract

In this work, we investigate the nanoparticle-cell wall interaction by NiO and mixed metal oxide CuO–NiO nanoparticles. We have synthesized and characterized the nanoparticles using XRD, FESEM, EDS, UV vis. spectroscopy, FTIR, Zeta, and TEM analysis in our previous work. Furthermore, a preliminary antibacterial study showed that both the nanoparticles performed very well as antibacterial agents. In this extended work, we investigate the mechanism of interaction of NiO and CuO–NiO nanoparticles with *S. aureus* and *E. coli* cells as there are number of studies for antibacterial mechanism of CuO nanoparticles. The uptake of crystal violet dye in the outer bacterial membrane, the release of ß-galactosidase enzyme, and relative electric conductivity assay were used to investigate changes in the permeability and integrity of the cell membrane. Superoxide ions, which are produced intracellularly as ROS by nanoparticles, severely damage bacterial membranes. Zeta potential measurement, which resulted in surface charge neutralization, proved membrane instability. FTIR analysis was used to identify changes in the proteins, carbohydrates, and fatty acids that make up the chemical composition of cell surfaces. AFM imaging demonstrated extensive alteration of the nanomechanical and surface characteristics. Confocal microscopy examination supported the DNA fragmentation and nanoparticle-cell adhesion. Due to their enhanced antibacterial activity when compared to monometallic oxide nanoparticles, this study demonstrated that mixed metal oxides can be employed in the health and biomedical sectors.

✉ Sudarsan Neogi
sneogi@che.iitkgp.ac.in

Debashri Paul
debashripaul@gmail.com

Ankur Pandey
pandeyankur111@gmail.com

[1] Indian Institute of Technology Kharagpur, Kharagpur, West Bengal 721302, India

[2] Indian Institute of Technology Guwahati, Guwahati, Assam 781039, India

Graphical abstract

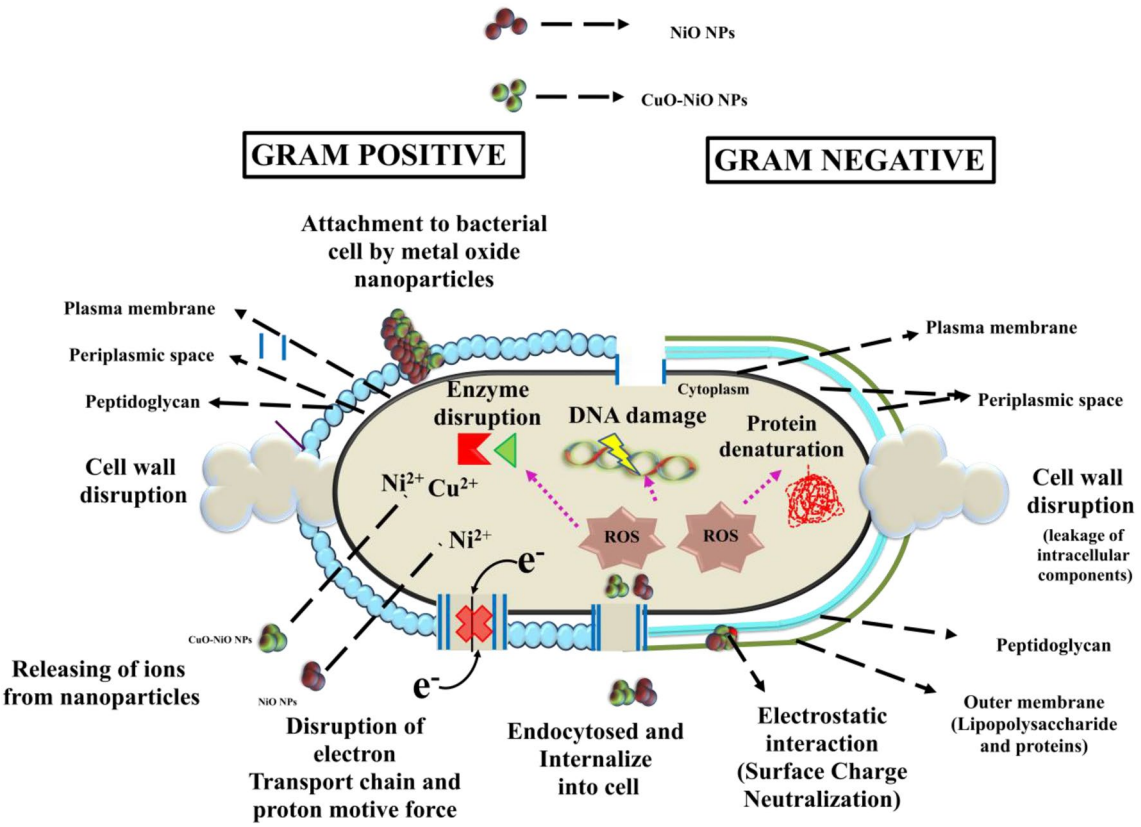

Keywords Nanoparticle-cell interaction · Antibacterial activity · FTIR spectroscopy · AFM analysis · Confocal microscopy

Abbreviation

AFM	Atomic Force Microscopy
BET	Brunauer–Emmett–Teller
BJH	Barrett, Joyner, and Halenda
CFU	Colony Forming Unit
DAPI	6-Diamidino-2-phenylindole
DNA	Deoxyribonucleic acid
EDTA	Ethylenediaminetetraacetic acid
FTIR	Fourier Transform Infra-Red
FESEM	Field Emission Scan Electron Microscopy
LB	Luria Bertani
LPS	Lipopolysaccharide
MBC	Minimum Bactericidal Concentration
MIC	Minimum Inhibitory Concentration
MMO	Mixed Metal Oxide
NBT	Nitroblue tetrazolium
ONP	O-nitrophenol
ONPG	Ortho-nitrophenyl-β-galactoside
PBS	Phosphate buffered saline
ROS	Reactive Oxygen sSpecies
UV–Vis	Ultraviolet–visible
XRD	X-Ray Diffraction

Introduction

The field of nanotechnology has been gaining importance because of its applications in various fields like electronics, catalysis, mechanics, water treatment, cosmetics, medicines, drugs and biomedical applications (Paul et al. 2020a; Ismail et al. 2019). Currently, bacterial resistance to antibiotics is increasing in an alarming rate. These antibiotic-resistant strains of both Gram-positive and Gram-negative microbes are a significant threat and concern to the global population. The indiscriminate use of antibiotics has led to the emergence of these antibiotic or drug-resistant strains. Hence, promising antibacterial agents such as metal oxide nanoparticles work on various strains, including drug-resistant microorganisms (Ko et al. 2012; Sirelkhatim et al. 2015; Morones et al. 2005; Azizi-Lalabadi et al. 2019; Widiarti et

al. 2017; Siddiqi et al. 2018; Tripathi and Goshisht 2022; Atri et al. 2023).

NiO nanoparticles have been used as an antimicrobial agent against different microbial strains like *Escherichia coli, Streptococcus pnemoniae, Escherichia hermannii, Staphylococcus aureus, Klebsiella pneumonia, Shigella dysenteriae,* and *Proteus vulgaris* (Lalithambika et al. 2017; Rahman et al. 2018; Angel Ezhilarasi et al. 2018; Ezhilarasi et al. 2016; Abbasi et al. 2019; Sabouri et al. 2019) where zone of inhibition was carried out to determine the antibacterial activity. NiO nanoparticles caused cellular damage (TEM analysis) of *Bacillus subtilis* and *Pseudomonas aeruginosa* strains. Another study showed that the generation of ROS (Reactive oxygen species) at NiO nanoparticle interface put oxidative stress on cell membrane, causing its damage and ultimately cell lysis (Behera et al. 2019).

A combination of two or more metal oxides can produce nanocomposite materials with unique physical and chemical properties. Also, these nanoparticles show enhanced due to the synergy between the metal oxides (John Owonubi et al. 2020). NiO based mixed metal oxide (MMO) nanoparticles have shown better antibacterial activity when compared to only NiO nanoparticles. CdO-NiO nanocomposites exhibited good antibacterial activity against foodborne pathogens and showed enhanced activity than NiO nanoparticles (John Owonubi et al. 2020). A similar result was seen for NiO-TiO_2 composite nanofibres (John Owonubi et al. 2020). NiO based trimetallic MMO also enhanced antibacterial activity (Paul et al. 2020b) and against various pathogenic bacterial strains (Karthik et al. 2018; Subhan et al. 2015).

A probable antibacterial mechanism has been established for CuO nanoparticles (Meghana et al. 2015; Applerot et al. 2012). Hence we do not focus in this work of already studied CuO antibacterial mechanism. There has been no significant study of the interaction between the bacterial cell surface and MMO nanoparticles. To our knowledge, a detailed study of nanoparticle-cell interaction has not been reported for NiO and MMO CuO–NiO nanoparticles. In our previous work (Paul and Neogi 2019), we used co-precipitation to synthesize NiO and CuO–NiO mixed metal oxide nanoparticles, which we then analyzed using a variety of methods. The tabular column includes the key findings. The NiO and CuO–NiO nanoparticles showed promising antibacterial activity against *S. aureus* and *E. coli* in an early evaluation of their antibacterial properties. The decrease in bacterial cell growth and the decline in colony-forming units served as evidence for this. A protein and nucleic acid leakage investigation and FESEM revealed that there was a leaking of intracellular components as a result of bacterial cell membrane rupture. The nanoparticle-cell interaction analysis for NiO and CuO–NiO nanoparticles is extended in the current paper. With the addition of NiO and CuO–NiO nanoparticles, the permeability of *E. coli*'s outer and inner membranes as well as the permeability of *S. aureus'* plasma and inner membranes were evaluated. Membrane instability was caused by the production of intracellular ROS like superoxide ions as well as a change in the surface potential of bacteria brought on by electrostatic contact. By using FTIR analysis, it is possible to determine how a nanoparticle interacts with the surface of a bacterial cell and how it culminates in damage to the cell's biomolecules. Using AFM, the ultrastructural characteristics such as cell length and height surface roughness were investigated, and confocal microscopy was used to examine DNA fragmentation.

Materials and methods

Experimental procedures of the assays given below are mentioned in detail in the supplementary file.

Characterization of nanoparticles

BET analysis and Raman spectroscopy analysis were used to further analyze the freshly produced nanoparticles. By applying the Brunauer–Emmett–Teller (BET) method with the Quantachrome AUTOSORB 1 equipment and nitrogen adsorption at 77.35 K on 250 mg of sample that had been degassed at 523 K for 5 h under high vacuum, the pore volume, average pore diameter, and surface area were calculated. The Barret-Joyner-Halenda (BJH) method was used to compute the average pore diameter, and the BET method was used to measure the specific surface area from nitrogen adsorption isotherms. Using a 532 nm laser beam, a Laser Micro-Raman system (HORIBA Scientific, LabRAM HR Evolution) was used to perform Raman spectroscopy on freshly produced nanoparticles.

Bacterial cell-nanoparticle interaction study

Outer membrane permeability by crystal violet assay

The outer membrane permeability of the *E. coli* and the plasma membrane permeability of *S. aureus* with the NiO and CuO–NiO nanoparticles were detected by treating damaged cells with a hydrophobic dye, crystal violet (Vaara and Vaara 1981; Sana et al. 2018). The detailed procedure is given in Supplementary File (section S2.2.1) The percentage of crystal violet uptake was expressed as follows (Halder et al. 2015):

$$\text{Percentage uptake of crystal violet} = (\text{OD value of sample} / \text{OD value of CV solution}) \times 100 \quad (1)$$

Inner membrane permeability by ONPG assay

The substrate employed to measure the bacterial strain's -galactosidase enzyme activity was O-nitrophenyl–D-galactopyranoside (ONPG). Understanding the inner membrane permeability of gram-negative bacteria (*E. coli*) and the plasma membrane permeability of gram-positive bacteria (*S. aureus*) cells led to the performance of this experiment (Ahmed et al. 2019). The detailed procedure is given in Supplementary File (section S2.2.2).

Permeability of cell membrane by relative conductivity assay

Relative conductivity assay was carried out according to method described by our previous work (Paul et al. 2020a). The detailed procedure is given in Supplementary File (section S2.2.3).

ΔL was calculated by.

$$\Delta L = L_3 - L_1 - L_2$$

where, L_2 is the electric conductivity of nanoparticles containing 5% glucose, while L_1 is the electric conductivity of isotonic bacteria solutions. L_3 is the isotonic bacterial solution with 5% glucose added and various nanoparticle concentrations. The control, L_0, is the conductivity of bacteria in 5% glucose treated in boiling water for 5 min. The percentage ratio revealed the relative electric conductivity of nanoparticles (Mei et al. 2013).

$$\text{Relative Electric Conductivity} = \left(\Delta L / L_0\right) \times 100 \quad (2)$$

Measurement of superoxide anion production

The Nitroblue Tetrazolium (NBT) Reduction Assay was performed in accordance with the Meghana et al. (2015) recommended protocol. The amount of superoxide anion present in the system directly correlates to the reduction of NBT to blue-colored formazan. To do this, sample solutions were created by varying the NiO concentration, and CuO–NiO nanoparticles were incubated with a 1×10^6 CFU/mL solution. The reaction mixture, which included 1 mL of phosphate buffer (50 mM), 200 mL of EDTA (12 mM), 1 mL of sample solution, and 1 mL of NBT (1%) was incubated at 37 °C for four hours. One set of samples was kept in the dark to serve as a blank, and the other set was illuminated for 120 s. The standard used was riboflavin (5 mg/mL), and all samples' absorbance was measured at 590 nm, and the results were compared.

Zeta potential analysis of bacterial cell membrane

S. aureus and *E. coli* bacterial strains were harvested from the early stationary phase by centrifugation (5000RPM, 10 min). The cells were washed twice with phosphate buffer (50 mM, pH 7.4) and the final concentration of 10^7 CFU/mL. The cells were subsequently exposed to NiO and CuO–NiO nanoparticle concentrations of 2 and 5 mg/mL. Finally, the treated and untreated cells were suspended in sterile phosphate buffer (50 mM, pH 7.4), and measurements of the -potential were taken utilizing a Zetasizer Nano-ZS-90 (Malvern Instruments, UK) (Ramalingam et al. 2016).

FTIR study of bacterial cell membrane damage

To further understand the changes taking place in the bacterial cell envelop, infrared spectra of the untreated cells, NiO, and CuO–NiO nanoparticles treated cells were recorded on a PerkinElmer (Model-Spectrum 100) spectrometer. FTIR spectroscopy, which produces a plot of % transmittance against wavenumber in the medium IR band, was used to record the functional groups and chemical bonds that were present on the surface. (4500–450 cm^{-1}). The detailed procedure is given in Supplementary File (section S2.2.6).

AFM analysis

The control bacterial cells and treated bacterial cells were analyzed using tapping mode of atomic force microscopy (AFM, Bruker, Innova series) which used a sharp-edged antimony doped silicon tips (TESPA-V2, Bruker). It Its specifications include 320 kHz frequency, 42 N/m force constant, and 0.01 to 0.025 Ω/cm resistivity. The scan frequency was held constant at 0.7–0.8 Hz. The "Nanoscope Analysis" software was used to evaluate the AFM pictures, line scan image analysis, and the root mean square roughness values. The root-mean-square (R_q) roughness of the bacterial cell exterior, which is determined by the following equation, was calculated from the AFM height images of samples (Li et al. 2015):

$$R_q = \sqrt{\frac{\Sigma(Z_{ij} - \overline{Z})^2}{N}} \quad (3)$$

where, Z_{ij} is the height value of each single point (nm), $\overline{Z}$ is the average height (nm) and N is the number of experimental points within the given area.

The detailed procedure for sample preparation is given in Supplementary File (section S2.2.7).

DNA fragmentation by confocal analysis

Nuclear DNA fragmentation of the bacterial cell was detected by staining the nuclei with 2.86 mM of DAPI. The detailed procedure is given in Supplementary File (section S2.2.8). The nanoparticle treated and untreated cells were placed on coverslips, and this was kept in the dark for 20 min. Finally, coverslips were mounted on the glass slide. The slides were visualized under a confocal microscope (ZEISS LSM 880) with an excitation wavelength of 358 nm.

Results

Some of the key findings and results of our previous work are given in Table 1.

Characterization of nanoparticles

Brunauer–Emmett–Teller (BET) Analysis and RAMAN spectroscopy of nanoparticles

The textural properties of the nanoparticles were evaluated using Brunauer–Emmett–Teller (BET) analysis. The nitrogen adsorption–desorption isotherm represents the category of type IV isotherm which indicates mesoporous structure for NiO and CuO–NiO nanoparticles mentioned in the IUPAC classification(Monga and Basu 2019; Sahoo et al. 2012) (Fig. 1(a1 and b1)). The slope of the isotherm increases from relative pressure 0.4 to 0.9, which reflects the mesoporous nature (Bepari et al. 2020). In the case

Table 1 Key Results of our previous work Paul and Neogi (2019)

	Characterization techniques and results obtained		
Technique	**Results NiO nanoparticle**	**Results CuO-NiO nanoparticle**	**Reference**
XRD analysis	Cubic phase of bunsenite	Monoclinic phase of CuO or tenorite and Cubic phase of NiO nanoparticles	Paul and Neogi (2019)
FESEM analysis	Spherical agglomerated particles	Spherical agglomerated particles	
UV–visible absorption spectroscopy	Absorption peak at 350nm Band gap energy: 3.17 eV	Absorption peak from 289nm-310nm. Band gap energy: 3.34 eV	
FTIR analysis	Peaks showed the formation of NiO nanoparticles	Peaks showed the formation of CuO-NiO nanoparticles	
TEM analysis	Spherical particles Particle size: 12 ± 4 nm (Fig. S1(a) and (c))	Spherical particles Particle size: 8 ± 2 nm (Fig. S1(b) and (d))	
Zeta Potential	pH= 6.5 ZP: 31.5 mV	pH= 6.5 ZP: 25.5 mV	
	Key results of antibacterial activity of NiO and CuO-NiO nanoparticles		
Growth curve analysis	exponential phase: early third hour stationary phase: end of seventh hour		Paul and Neogi (2019)
CFU reduction study	*84% reduction in CFU (E. coli)*	*94% reduction in CFU (E. coli)*	
Inhibition study (5m/mL NP conc.) (Release of ions mg/mL)	**Released metal ion concentration (mg/mL) (Ni^{2+})** Time (hours) / *S. aureus* / *E. coli* 2 / 0.99 / 0.45 8 / 1.26 / 1.16	**Released metal ion concentration (mg/mL) (Cu^{2+}, Ni^{2+})** Time (hours) / *S. aureus* / *E. coli* 2 / 0.38, 0.14 / 0.39, 0.14 8 / 0.66,0.323 / 0.49,0.295	
MIC/MBC	Bacterial concentration: 1 X 10^6 CFU/mL		
	MIC for *E. coli*: 8.5 mg / mL MIC for *S. aureus:* 6.7 mg / mL MBC for *E. coli*: 14.5 mg / mL MBC for *S. aureus:* 12 mg / mL	MIC for *E. coli*: 4.9 mg / mL MIC for *S. aureus:* 3.0 mg / mL MBC for *E. coli*: 7.8 mg / mL MBC for *S. aureus:* 5.0 mg / mL	
FESEM	Bacterial cells have undergone morphological changes (additional images in file Supplementary S3.2.7, Fig. S2)		
Cell integrity analysis	Leakage of nucleic acid and proteins		

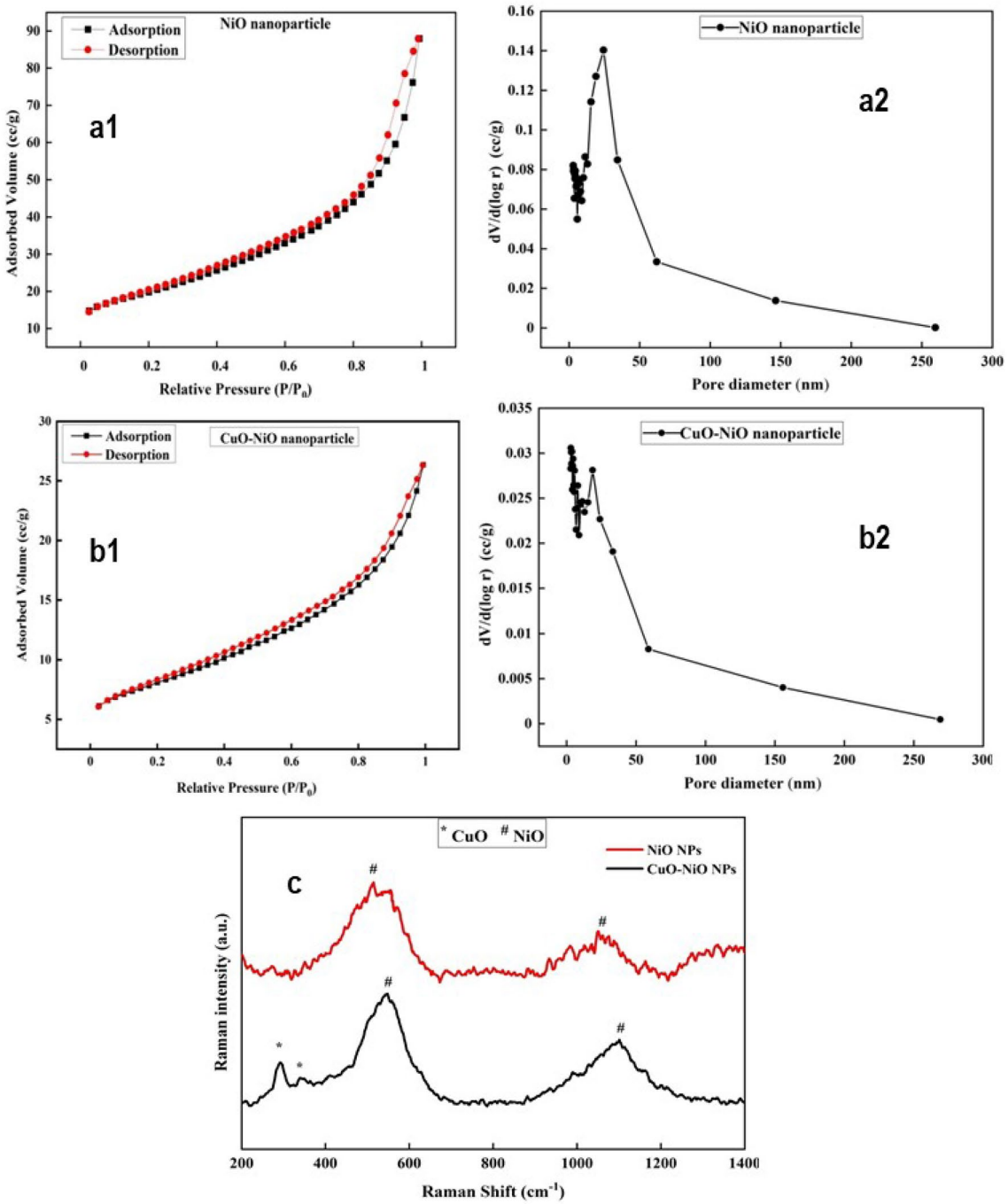

Fig. 1 N_2 adsorption–desorption isotherms of **a1** NiO nanoparticles and **b1** CuO–NiO nanoparticles. The mesopore size distribution curve of **a2** NiO nanoparticles and **b2** CuO–NiO nanoparticles. **c** Raman spectroscopy of NiO and CuO–NiO nanoparticles

of pore-size distribution plot, which is given in Fig. 1(a2 and b2), we observed that some pores exist at higher range value (> 50 nm). This also affects the surface area of both the samples. The surface area, pore diameter, average pore volume of NiO nanoparticles are 69.252 m^2/g, 7.86 nm and 0.14 cc/g; and for CuO–NiO nanoparticles are 28.450 m^2/g, 5.72 nm and 0.048 cc/g respectively.

The first-order longitudinal optical (1LO) and second-order longitudinal optical (2LO) phonon modes, respectively, have peak values for NiO nanoparticles at 514 and 1050 cm^{-1}. With a minor peak shift, as shown in Fig. 1c, the longitudinal optical modes of CuO at 540 and 1090

and the A_g and B_g modes of CuO at 293 and 340, respectively, appear together for CuO–NiO nanoparticles. This supports our prior XRD analysis findings and establishes the production of bimetallic MMO nanoparticles. (Kumar et al. 2020; Vivek et al. 2020; Wang et al. 2013).

Bacterial cell-nanoparticle interaction study

Outer membrane permeability by crystal violet assay

In the undamaged or normal cells, crystal violet's penetration ability is poor, but with membrane lesions, there is an uptake or entrapment of the dye in the cell (Guo et al. 2016; Khan et al. 2017). The uptake for damaged *E. coli* and *S. aureus* after CuO–NiO nanoparticles treatment was 55% and 62%, respectively, as seen in Fig. 2b. For NiO nanoparticles, the uptake was more for *E. coli* cells with an entrapment percentage of 55%, and for S. *aureus* was 49% (Fig. 2a). This showed that NiO damaged *E. coli* cells and uptake of the dye was faster than S. *aureus* strains and vice versa for CuO–NiO nanoparticles. However, the uptake of crystal violet by *S. aureus* and *E. coli* was 15% and 13%, respectively, in the absence of nanoparticles. The uptake of crystal violet by the strains shows there is an alteration in the bacterial cell membrane.

Inner membrane permeability by ONPG assay

The enzyme β-galactosidase, often used as a stress marker, is present in the cytoplasm of *E. coli* and *S. aureus*. β-galactosidase can leak outside the cell membrane only when there is cell damage. Hence, the detection of this enzyme is a crucial aspect of understanding cell membrane permeability. When both the nanoparticles damage the cytoplasm of *E. coli* and *S. aureus,* β-galactosidase catalyzes the hydrolysis of substrate ONPG to produce ONP given in Eq. (4), and this was determined by measuring the OD420 using UV vis spectroscopy(Mei et al. 2013; Saito et al. 2019).

The absorbance values were significantly less even after 6 h for untreated bacterial cells as there is a negligible release of the enzyme into the solution, as seen in Fig. 2(c) and (d). S. *aureus* strains treated with MBC concentration of all NiO and CuO–NiO nanoparticles; it was seen that there was an increase in the absorbance of ONP from the early log phase (2 h). The absorbance increased up to 5 h and reached almost constant. A similar trend was seen for *E. coli,* but the absorbance of ONP increased more than S. *aureus* strains drastically after the first hour. A possible explanation could be that the thick peptidoglycan layer in *S. aureus* may initially reduce the enzyme's permeability. A similar result was observed when *E. coli* and *S. aureus* were treated with ZnO nanoparticles and monocaprylin(Deng and Zeng 2018).

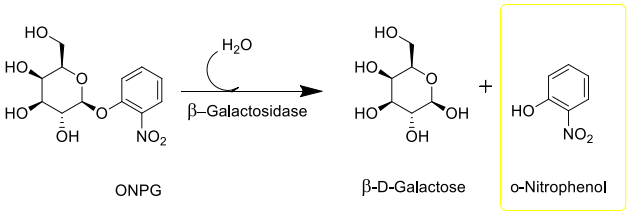

(4)

Permeability of cell membrane by relative conductivity assay

Another assay to relate the antibacterial activity and bacterial cell permeability of *S. aureus* and *E. coli* treated NiO and CuO–NiO nanoparticles is the relative electric conductivity assay. The figure show that the untreated cells have a low percentage relative conductivity value due to the normal cell lysis and cell death. Small ions like K^+, Na^+, and H^+ are not permeated outside the cytoplasmic membrane of undamaged bacteria. This is sustained due to the structure and chemical composition of the surface. When the cells were treated with CuO–NiO nanoparticles (Fig. 2f), it was observed that with an increase in the concentration of nanoparticles, the percentage relative conductivity in the suspension increased rapidly. This indicated that with increased bacteria permeability, there is a more significant loss of electrolytes into the suspension (Patra et al. 2015; Zhang et al. 2020). With an increase in the concentration of the nanoparticles, the relative conductivity of the suspension containing *S. aureus* was more than that of *E. coli*. But *E. coli* strains showed more percentage relative conductivity than *S. aureus* when treated with NiO nanoparticles (Fig. 2e). However, from both the graphs, it is evident that NiO and CuO–NiO nanoparticles increase the cell membrane permeability. When concentration of nanoparticles increased, MMO nanoparticles had a greater release of electrolytes from both the bacterial strains than mono metallic NiO nanoparticles.

Measurement of superoxide anion production

Treatment of bacterial strains with NiO and CuO–NiO nanoparticles generated oxidative stress due to the production of superoxide anions. As seen in Fig. 3a, with an increase in the concentration of nanoparticles, the absorbance increased, indicating a significant formation of blue formazan, which also meant an increase of $O_2^{\cdot-}$ in the cytoplasm of *E. coli* and *S. aureus* bacterial strains. The nanoparticles stimulated the formation of $O_2^{\cdot-}$ anions and this possibly increased the oxidative stress. The intracellular ROS production caused DNA damage and cellular damage and could trigger cell apoptosis (Meghana et al. 2015; Giannousi et al. 2014). Riboflavin (5 mg/mL) was used as the standard. It was observed that with an increased concentration of nanoparticles, CuO–NiO

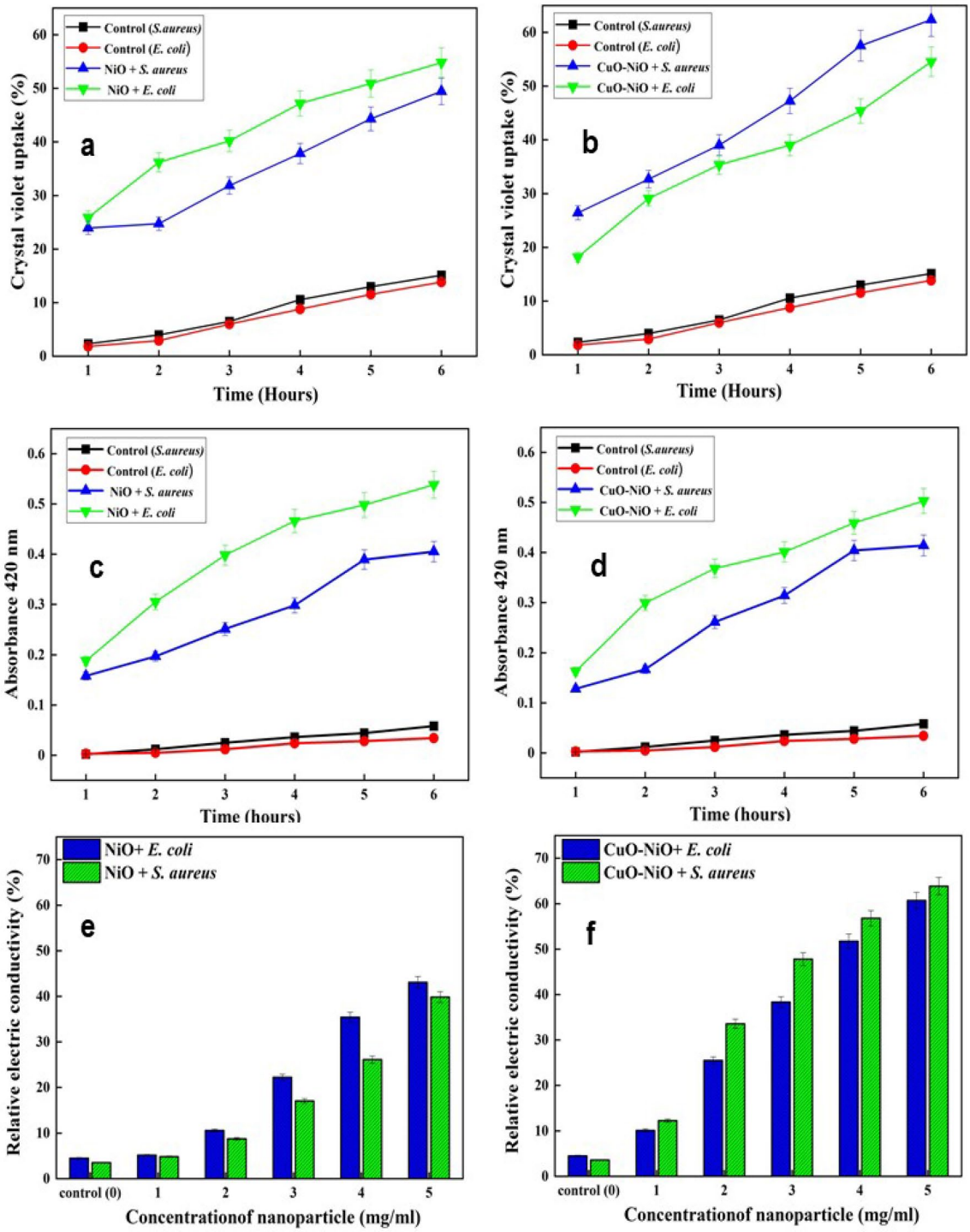

Fig. 2 Crystal violet assay of *S. aureus* and *E. coli* treated with **a** NiO and **b** CuO–NiO nanoparticles. ONPG assay of *S. aureus* and *E. coli* treated with **c** NiO and **d** CuO–NiO nanoparticles. Relative Electric conductivity of *S. aureus* and *E. coli* treated with **e** NiO and **f** CuO–NiO nanoparticles

nanoparticles generated greater superoxide anions compared to NiO nanoparticles.

Zeta potential analysis of bacterial cell membrane

The measurement of the ζ-potential is an important aspect in comprehending how surface neutralization results in

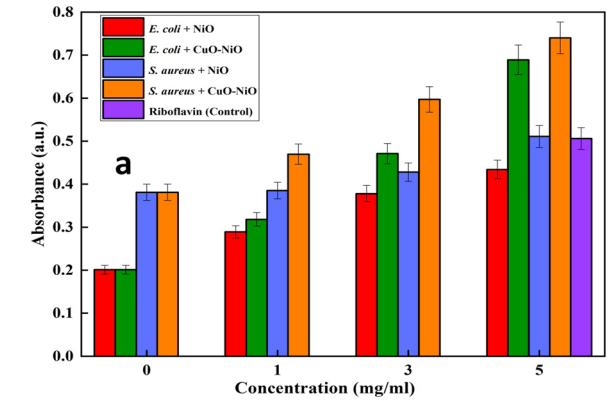

b

Concentration of nanoparticle (mg/ml)	*S. aureus* (Z.P. mV)		*E. coli* (Z.P. mV)	
	NiO	CuO-NiO	NiO	CuO-NiO
2	-23.6	-23	-33.7	-31.1
4	-21.6	-18.6	-23.6	-21.8

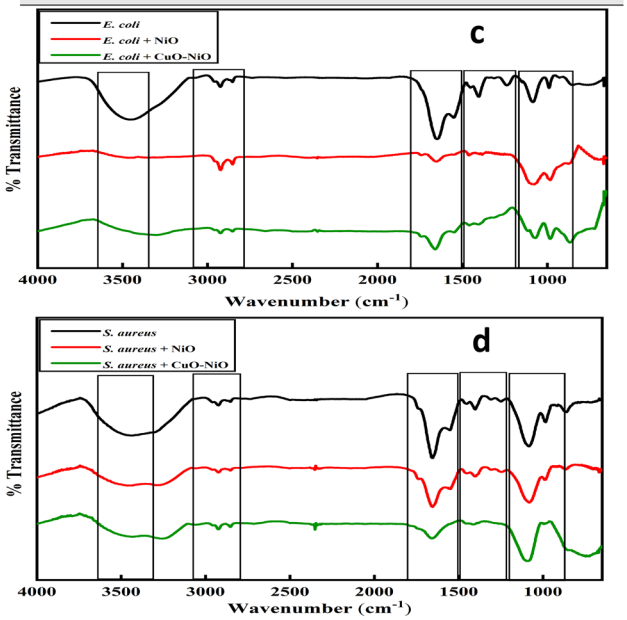

Fig. 3 **a** Intracellular O_2^- generated by NiO and CuO–NiO nanoparticles in *E. coli* and *S. aureus* bacterial strains **b** Zeta potential of bacteria treated with nanoparticles. FTIR spectrum of *S. aureus* and *E. coli* treated with **c** NiO and **d** CuO–NiO nanoparticles

membrane damage. The untreated strains of *E. coli* and *S. aureus* were found to have average Zeta potentials of 42.0 and 32.6 mV, respectively. Due to excessive amounts of lipopolysaccharide (LPS) in the cell's outer membrane, gram-negative bacterial strains have a higher negative charge than Gram positive bacterial strains. (Arakha et al. 2015). It is explicit from Fig. 3b that the zeta potential changes when the strains' negative surface potential is combined with the positive surface potential of NiO and CuO–NiO nanoparticles. At 2 mg/mL, the ζ-potential changes only slightly, but at 4 mg/mL, the zeta potential changes by a higher percentage, indicating a shift towards neutrality. Compared to *S. aureus* cells, *E. coli* cells showed a shift significantly. It might be because the electrostatic attraction of the cationic nanoparticles has been observed to disrupt the lipopolysaccharide barrier in Gram-negative bacteria, causing damage to the membrane structure (Ramalingam et al. 2016; Halder et al. 2015). The change in ζ-potential had caused membrane permeabilization and this can be correlated with crystal violet assay and ONPG assay, with the uptake of crystal violet dye and detection of ONP, respectively.

FTIR study of bacterial cell membrane damage

The bending and stretching vibrations of functional groups present in the cell wall of bacterial strains like proteins, nucleic acid, lipopolysaccharides, lipid, sugar, etc., can be identified by FTIR spectroscopy. As seen in Fig. 3c and d, the spectrum is divided into five regions.

Region 1 (3600–3200 cm^{-1}): for untreated *E. coli* and *S. aureus* bacterial strains, the broad range between 3550 and 3200 cm^{-1} is connected with the amide region. When *E. coli* was treated with NiO and CuO–NiO NPs, the peaks in the area disappeared. For damaged *S. aureus* strains, the intensity of peaks was reduced (Ramalingam et al. 2016).

Region 2 (3100–2600 cm^{-1}): the spectral band of this region indicates the fatty acid region. The absorption peaks for (C–H) asymmetric stretching of CH_3 in fatty acids, (C–H) asymmetric stretching of CH_2 in fatty acids, (C–H) symmetric stretching of CH_3 in fatty acids was observed at 2959, 2926 and 2854 cm^{-1} respectively for *E. coli* strains. The same was observed at 2961, 2928 and 2851 cm^{-1}, respectively for *S. aureus* strains (Ramalingam et al. 2016; Davis and Mauer 2010; Faghihzadeh et al. 2016). The disappearance of the methylene stretching peaks was observed at 2959 cm^{-1} and a reduction of peak intensity at 2926 cm^{-1} and 2854 cm^{-1} for *E. coli* when treated with NiO and CuO–NiO NPs. A similar change was observed in the alteration of the fatty acid-tail structure of damaged *S. aureus.*

Region 3 (1800–1500 cm^{-1}): includes protein region dominated by amide I and II proteins. For *E. coli* and *S. aureus,* a broad region from 1695 to 1635 cm^{-1} indicates the amide I band of α and β helical structure of proteins. Amide II bands appear between 1550 and 1530 cm^{-1} region. The peak at 1746 cm^{-1} represents > C=O stretching in lipid ester(Kumar et al. 2020; Davis and Mauer 2010; Devi et al. 2010; Amna et al. 2013). When *E. coli* treated with NiO NPs, there was a sharp decrease in peak intensity at 1651 cm^{-1} and 1537 cm^{-1}. *E. coli* treated with CuO–NiO NPs reduction of peak intensity occurred at 1649 cm^{-1} and 1542 cm^{-1}. The peak shift and decrease in intensity indicated the changes occurring in amide groups present in phospholipids. A peak

shift appeared at 1654 cm^{-1} and 1539 cm^{-1} when *S. aureus* was treated with NiO NPs towards the lower wavenumber. For CuO–NiO NPs, peak intensity reduction at 1650 cm^{-1} and 1549 cm^{-1} the peak disappeared. This clearly indicated the alteration of protein structure.

Region 4 (1500–1200 cm^{-1}): The bonds of proteins, nucleic acids, fatty acids and phosphate compounds exist in this region. 1470–1450 cm^{-1} band indicated the –CH band of $>CH_2$ in lipids and proteins. 1400 cm^{-1} indicated C=O symmetric stretching of COO^- groups in amino acids, fatty acids. The region 1300–1320 cm^{-1} represented the amide III band in proteins. The band 1248 cm^{-1} indicated the P=O asymmetric stretching of phospholipids and teichoic acid for *S. aureus* strains (Davis and Mauer 2010; Qu et al. 2016; Kiwi and Nadtochenko 2005; Naumann 1984). When *E. coli* treated with NiO and CuO–NiO NPs, the majority of the peaks disappeared in this region except for a small peak at 1461 cm^{-1}, indicating the release of proteins and nucleic acid. There was a reduction in the intensity of peaks when *S. aureus* was treated with NiO NPs, and the peaks disappeared when treated with CuO–NiO NPs. The release of intracellular ROS can lead to damage and change of wavenumber in the fatty acid region.

Region 5 (1200–800 cm^{-1}): constitute the carbohydrates and fingerprint region. 1200–900 cm^{-1} indicate the C–O–C, C–O dominated ring vibration in polysaccharides while 1085 cm^{-1} represented the P=O symmetric stretching in DNA, RNA and phospholipids (Faghihzadeh et al. 2016; Jiang et al. 2004; Noman et al. 2019). Below 900 cm^{-1} up to 600 cm^{-1} constituted the fingerprint region. After NiO and CuO–NiO NPs treatment of *E. coli*, the peaks appeared at 1095, 966, 866 cm^{-1} and 1061, 976, 871 cm^{-1} respectively. There were peak shifts and reduction in peak intensity for both cases. For damaged *S. aureus,* peaks were observed at 1079, 978, 868 cm^{-1} after NiO treatment and at 1084 cm^{-1} after CuO–NiO treatment. The peaks at the fingerprint region correspond to unique weak bands of nucleic acid. There were changes observed, and peak shifts appeared in this region for both the treated cells. This region, along with region 4, indicated the pit formation within the strains.

AFM analysis

AFM analysis was carried out to understand the ultrastructural and cell alteration properties of the bacterial cells after treatment with NiO and CuO–NiO nanoparticles (Mathelié-Guinlet et al. 2018). Two dimensional AFM images of the control bacteria *E. coli* and *S. aureus* [Fig. 4(a1 and d1)] shows typical rod-shaped and spherical shaped cell, respectively. The surface was relatively smooth without any alterations or membrane perturbations. Control *E. coli* [Fig. 4 (a1)] and *S. aureus* [Fig. 4 (d1)] had an average cell size of 2.04 µm (length) and 0.8 µm (diameter) respectively. Also, from the line scan, Fig. 4(a2 and d2), it is evident the bacterial cell surface is quite smooth without much variation in Z-height and the average height of control bacteria *E. coli and S. aureus* are 216 nm and 203 nm respectively. After incubation with the nanoparticles there was change in surface morphology of the strains. When *E. coli* cells were treated with CuO–NiO nanoparticles, there is alteration of the morphology of the bacterial cell wall with rupture and deformation. Also, there was a decrease in size of the strain i.e., from 2.04 to 1.07 µm as well a reduction in the average height of the strain, from 216 to 84 nm. This can be seen in the line scan image along with groove formation in the graph Fig. 4(c1 and c2). The line scan indicates the variation of stiffness of the cell wall along the cell. The increase in surface roughness indicated the difference between membranes before and after the treatment with CuO–NiO nanoparticles. Surface roughness of the control bacteria *E. coli* and CuO–NiO nanoparticles treated *E. coli* cells were 17.60 nm and 35.04 nm respectively. This increase demonstrated the membrane damage of the cell. Similar results were obtained when *E. coli* cells were treated with NiO nanoparticles which are given in the Table 2 and graph Fig. 4(b1 and b2). *S. aureus* treated by CuO–NiO nanoparticles showed similar cell membrane damage with the decrease in size of the cell and average height Fig. 4(e1 and e2). *S. aureus* treated by NiO nanoparticles showed an elongation of the cell size, however the damage was certain Fig. 4(f1 and f2). An increase in surface roughness was observed when *S. aureus* was treated with both the nanoparticles (Table 2). Increase of surface roughness of *E. coli* and *P. aeruginosa* after silver nanoparticle treatment was reported by Ramalingam et. al (Ramalingam et al. 2016). The groove formation and ruptured ultrastructure of *E. coli* and *S. aureus* was observed by Jin et al (Jin et al. 2010). The cell debris, attachment of nanoparticle to cell wall and deformed bacterial cell membrane was observed in the AFM images which were also confirmed previously by our FESEM analysis (3D AFM images are given in section S3.2.7, Fig. S2).

DNA fragmentation by confocal analysis

E. coli cells suffered an irreversible damage which was seen by the structural changes in confocal fluorescence microscopy of cells after nanoparticle treatment. Fluorescent dye DAPI was employed to stain the cells in order to assess DNA structural damage because it selectively binds the DNA of bacteria. (Mathelié-Guinlet et al. 2018). A cell membrane that is unharmed or intact can let DAPI through. As a result, both live and dead cells are stained. Untreated *E. coli* cells had a homogeneous rod-like structure and

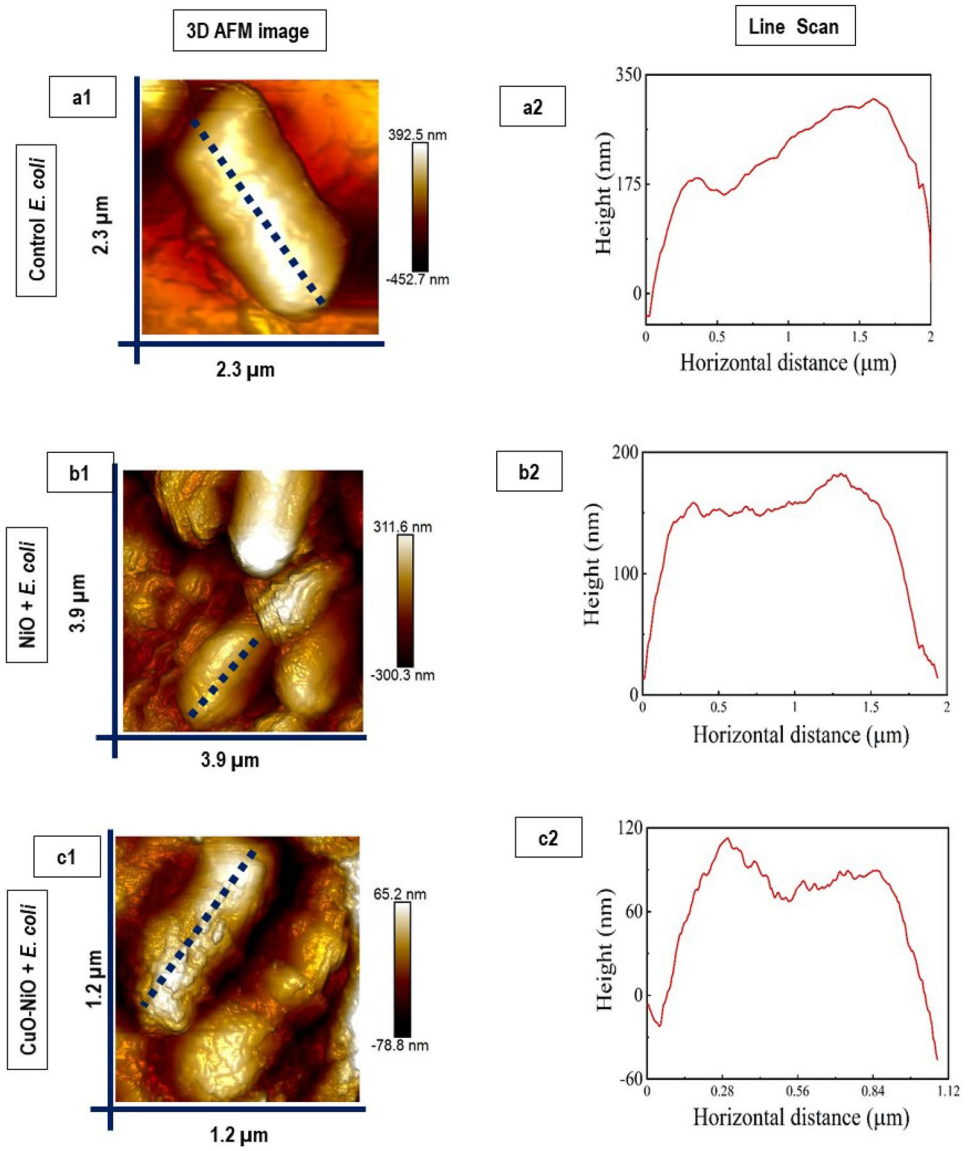

Fig. 4 2D AFM images of **a1** control *E. coli* **b1** NiO + *E. coli* **c1** CuO–NiO + *E. coli* **d1** control *S. aureus* **e1** NiO + *S. aureus* **f1** CuO–NiO + *S. aureus*. Line scan of AFM images of **a2** control *E. coli* **b2** NiO + *E. coli* **c2** CuO–NiO + *E. coli* **d2** control *S. aureus* **e2** NiO + *S. aureus* **f2** CuO–NiO + *S. aureus*

a smooth surface, as shown in Fig. 5(a1 and a2), but the fluorescent pictures in Fig. 5(b2 and c2) clearly show DNA damage and fragmentation. Also evident in the bright field pictures of Fig. 5(b1) and c1 is the attachment of NiO and CuO–NiO nanoparticles to the bacterial cell that has been damaged. Figure 5(a3, b3 and c3) show the merged field images. A similar observation is seen in the *S. aureus* bacterial cells when treated with the nanoparticles (section S3.2.8 Fig. S3). The images are given in Supplementary file.

Discussions

In our earlier research, co-precipitation method was used to synthesize NiO and CuO–NiO nanoparticles. We used a variety of techniques to characterize the nanoparticles. According to our earlier research, NiO and CuO–NiO nanoparticles effectively combatted *E. coli* and *S. aureus* strains by reducing the number of bacterial colonies (CFU reduction study) and their growth curves. Strain damage and nanoparticle adhesion to the cell wall was visible in FESEM pictures. Proteins and nucleic acids were released from the broken membrane, according to the cell integrity study. Ions were released, which inhibited the rate of bacterial growth. The concentration of the nanoparticles also impacts how they interact with different bacterial strains (Paul and Neogi 2019). Additionally, CuO–NiO nanoparticles demonstrated greater antibacterial action against *S. aureus* strains than *E. coli* strains, and the opposite was true for NiO. A similar observation was seen for CuO nanoparticles by Javadhesari et al. (Moniri Javadhesari et al. 2019) and for NiO nanoparticles by Wang et al. (Wang et al. 2010).

Fig. 4 (continued)

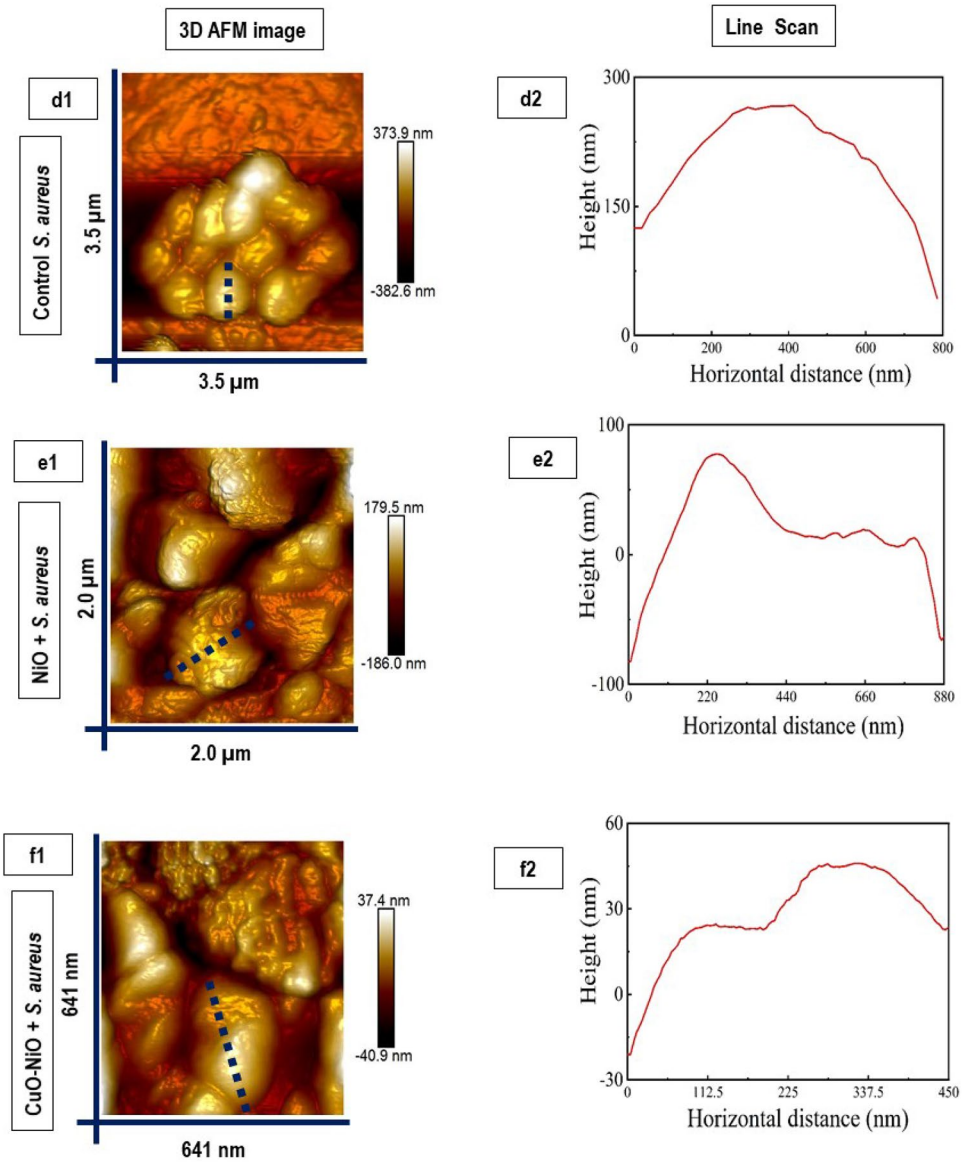

Table 2 Size, average height and Root mean square roughness of *S. aureus* and *E. coli* treated with NiO and CuO–NiO nanoparticles

Sample	Size (µm)	Average height (nm)	Root mean square roughness (R_q) (nm)
Control *E. coli*	2.04	216	17.60
E. coli + NiO	1.94	135	25.55
E. coli + CuO–NiO	1.07	64	35.04
Control *S. aureus*	0.80	203	14.13
S. aureus + NiO	0.87	23	30.51
S. aureus + CuO–NiO	0.45	28	23.08

NiO and CuO–NiO nanoparticles caused a membrane rupture and destruction of the cell membrane, which caused cell lysis in both strains. This interaction of nanoparticle-cell wall was studied in our present work. Crystal violet assay confirmed the outer membrane permeability and ONPG assay confirmed the inner membrane permeability of *E. coli* strain. Also, it confirmed the plasma membrane permeability for *S. aureus* strains. When the strains were treated with an increasing concentration of nanoparticles, the permeability of the membrane was increased. The percentage relative conductivity of the cell suspension increased because of the leakage of the small ions or electrolytes (Sana et al. 2018; Ahmed et al. 2019; Zhang et al. 2020).

The antibacterial mechanism of CuO nanoparticles have been observed as the following by the researchers: (Applerot et al. 2012) have stated based on their research that copper and endogenous H_2O_2 react to produce hydroxyl and superoxide radicals. The damage to the bacterial cell membrane was mediated by the presence of

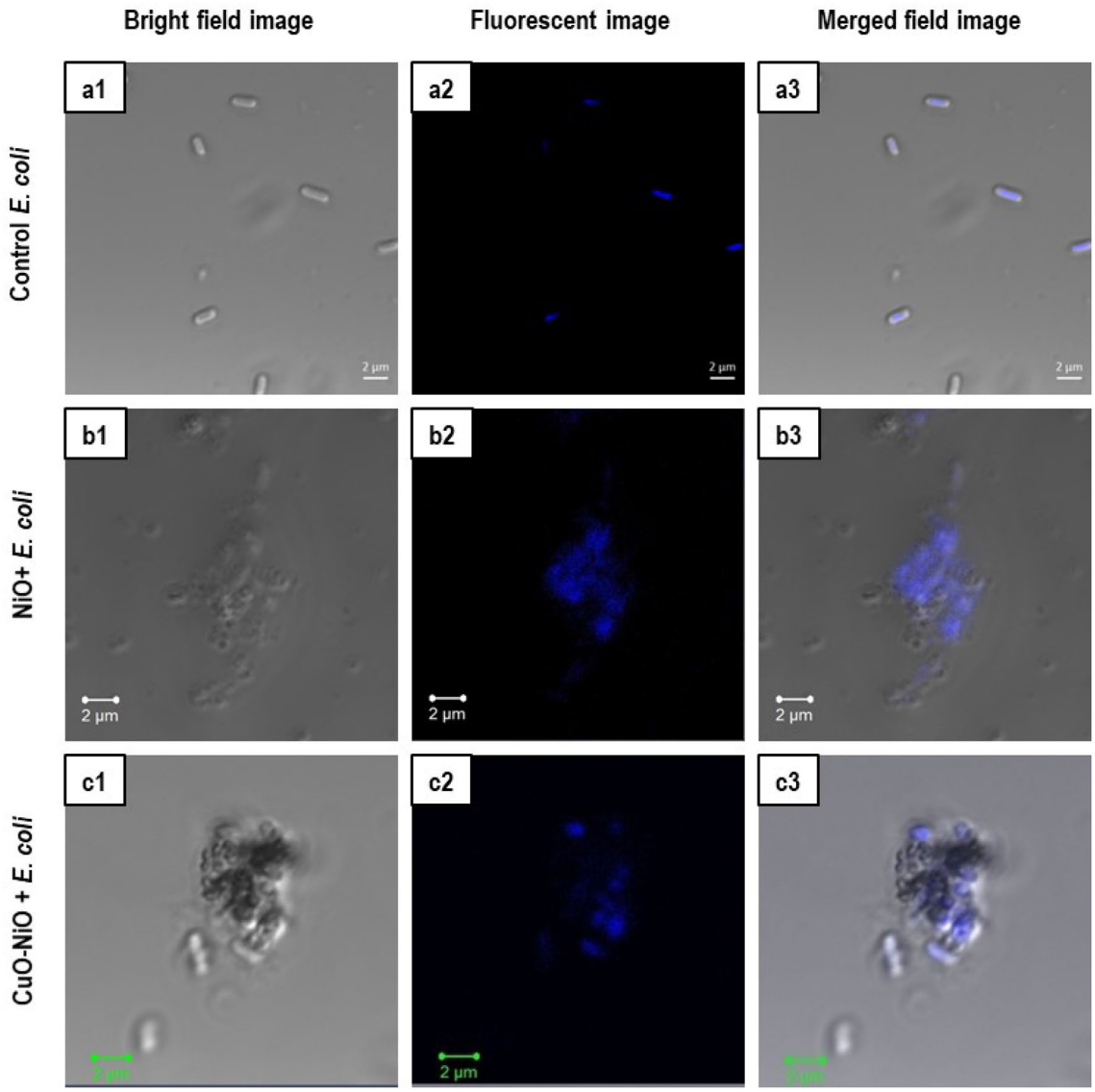

Fig. 5 Bright Field images of **a1** control *E. coli* **b1** NiO + *E. coli* **c1** CuO–NiO + *E. coli* Fluorescent images of **a2** control *E. coli* **b2** NiO + *E. coli* **c2** CuO–NiO + *E. coli*. Merged field images of **a3** control *E. coli* **b3** NiO + *E. coli* **c3** CuO–NiO + *E. coli*

harmful O_2^- anions due to the cell attachment or internalized CuO nanoparticles. The bacterial cell membrane suffered oxidative damage as a result of the interaction between nanoparticles and the cell membrane which was confirmed by (Meghana et al. 2015).

The bactericidal nature of NiO nanoparticles, the interaction of these nanoparticles with the cell wall of *E. coli* and *S. aureus* strains can follow any of these plausible sequences:

The electrostatic force of attraction is dependent on the surface area available for interaction. NiO nanoparticles has a high zeta potential value. Hence the first pathway of interaction could be surface charge neutralization of cell membrane due to electrostatic interaction and internalization of NiO NPs. The attachment caused a disruption of the membrane wall.

The attachment of NP to bacterial cell membrane releases Ni^{2+}, which inhibits the bacterial growth rate and becomes toxic to the cell seen in this study. (Wang et al. 2010) similarly observed that there is an intracellular release of Ni^{2+} ions, which interfered with the intracellular Ca^{2+} metabolism. This was the Nano Trojan Horses mechanism for nanoparticle toxicity, wherein nanoparticles can enter cells was the suggested mode for nanoparticle toxicity by (Horie et al. 2009).

The generation of superoxide ions was observed, which was not significant as CuO–NiO nanoparticles for the same concentration of nanoparticles. Since the ROS generation

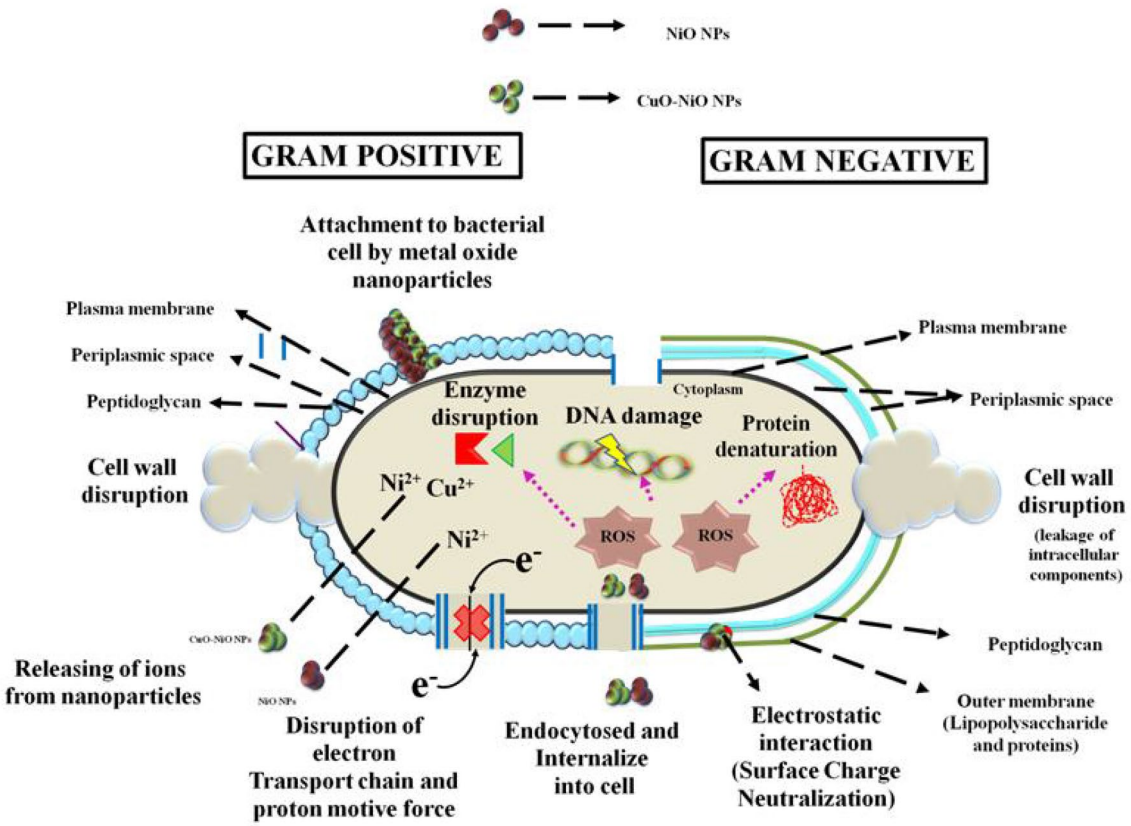

Fig. 6 Schematic representation of nanoparticle-cell wall interaction of NiO and CuO–NiO nanoparticles against *E. coli* and *S. aureus*

is relatively less as NiO is a less redox active element than copper, it failed to show enhanced activity like CuO–NiO nanoparticles.

However, at MBC concentration, bacterial cell death was evidenced. So, the combined action of adherence of nanoparticles to the wall and ROS generation can be considered as the primary mechanism where membrane ruptured, resulting in cell death because cellular glutathione was oxidized by metal ions discharged from NiO-NPs. The imbalance in oxidants and antioxidants resulted an oxidative stress within the microbes. The excess generation of ROS within the bacterial cell led to the disruption of the antioxidant enzyme activities.

The bactericidal nature of CuO–NiO nanoparticles, the interaction of these nanoparticles with the cell wall of *E. coli* and *S. aureus* strains can follow any of these plausible sequences:

Ni^{2+} and Cu^{2+} ions are released when nanoparticles interact with the bacterial cell membrane, which slows down the growth of the bacteria (Wang et al. 2010). CuO–NiO nanoparticles suppressed bacterial growth more effectively than NiO nanoparticles because they included both ions (Kung et al. 2017). Metal ions released by CuO–NiO NPs oxidized cellular glutathione, which excessively generated ROS. Oxidative stress can harm cells when there is an excess production of intracellular ROS (Meghana et al. 2015; Hou et al. 2017). Additionally, many enzymes and proteins' -SH groups (thiol groups) become inactive when these ions interact with them.

Since copper is a redox active element, it can take part in both oxidation and reduction processes. For instance, the Fenton reaction may be used to catalyze the reduction of cuprous ions by superoxide radical anions to create biologically damaging hydroxyl radicals as seen by (Jomova et al. 2012). Also, MMO nanoparticles have more surface defects than pure metal oxide nanoparticles. The combined action of adherence of nanoparticle to the wall, intracellular ROS generation due to the clearance of glutathione pool, greater ROS generated on particles' surface, internalization of small sized nanoparticles into the membrane resulted in enhanced antibacterial activity of MMO nanoparticles.

The positive zeta potential of nanoparticle surface caused an electrostatic interaction between the negative surfaces of bacterial strain wherein the surface charge of bacterial surface shifted towards neutrality (Halder et al. 2015). FTIR analysis of the cells showed the presence of various functional groups like carboxyl, hydroxyl, amide and phosphate groups. FTIR spectra of treated bacteria cells when

compared to untreated cells suggest the change in peak intensity and disappearance of peaks which contain phosphate groups indicating the leakage of DNA, RNA; the damage of peptidoglycan and phospholipids of Gram-negative cell and the damage of peptidoglycan and teichocic acids of Gram positive cell. Alteration of amide I, II and III bands suggest the change in protein structure due to damage of the membrane and leakage of intracellular components. The change in vibration methyl group of membrane fatty acids and degradation of membrane carbohydrate moieties and fatty acids indicated the cell decomposition when treated with NiO and CuO–NiO nanoparticles.

Earlier studies of FESEM, AFM and bright field images of confocal, it was evident there was a change in cell surface morphology. AFM images revealed the smooth surface of untreated cells and the increased surface roughness values were observed when the cells were damaged by nanoparticles. The cells underwent shrinkage, reduction in vertical height and pit formation was evident. Nanoparticle attachment, cell debris formation and leakage of intracellular components were observed in FESEM and bright field images of confocal study. The DNA damage, loss and fragmentation are evident from the fluorescent images of confocal study.

An attempt to understand the antibacterial activity or nanoparticle-cell wall interaction of nanoparticles is seen in Fig. 6. CuO–NiO nanoparticles have shown promising and better antibacterial results than NiO against *E. coli* and *S. aureus* strains. Hence, mixed metal oxides can be used as antibacterial against various multidrug resistant strains.

Conclusions

This paper establishes the bacterial cell-nanoparticle interaction of NiO and CuO–NiO nanoparticles against *E. coli and S. aureus*. The nanoparticles had caused a membrane disruption. The release of intracellular components like nucleic acid, proteins, K^+ leakage, and the enzyme β-galactosidase confirmed the loss of cellular integrity and external structure. CuO–NiO MMO showed enhanced antibacterial activity compared to NiO nanoparticles. The release of ions from the nanoparticles can trigger intracellular ROS generation, which resulted in cell death. Zeta potential analysis confirmed the membrane destabilization. AFM analysis showed the nanomechanical and ultrastructural properties of cell surface and gave a clear understanding of the morphological changes undergone by the strains when treated with nanoparticles. The fragmentation of DNA and nanoparticle-cell attachment was confirmed by confocal microscopy analysis. FTIR analysis confirmed the changes and destruction of the functional groups present in the bacterial cell membrane when treated with both the nanoparticles. Presence of both the metals enhanced the antibacterial activity, and hence multi-metal oxides can be used as antibacterial agents against various multi-drug resistant strains. Thus, the results indicated that the monometallic metal oxide and mixed metal oxides could be used in various biomedical applications involving drug-membrane interactions.

Supplementary Information The online version contains supplementary material available at https://doi.org/10.1007/s11274-023-03712-2.

Acknowledgements The authors acknowledge the Department of Chemical Engineering, IIT Kharagpur for providing technical and financial support in the form of a research grant (as this work is a part of Doctoral thesis to IIT Kharagpur). The authors thank Prof. Dipankar Bandyopadhyay and the Centre for Nanotechnology, Indian Institute of Technology Guwahati, Assam, 781039, India their assistance in carrying out imaging analysis experiments. Also, the authors thank Mr. Jahar Mahala and Mr. Dhruba Sakha (IIT Kharagpur), Miss. Reena Dey, Dr. Srirupa Bhattacharyya and Dr. K. Dharamalingam (IIT Guwahati) for their invaluable assistance in the reported work. We also thank MeitY—grant no. 5(9)/2012-NANO for financial aids.

Author contributions DP and SN contributed to the conception and design of the experiments. DP performed the research. DP and AP analyzed the data. Imaging/Analytical tools: AP. DP wrote the manuscript. SN is the paper supervisor.

Funding Not Applicable.

Data availability All data generated or analyzed during this study are included in this published article.

Declarations

Conflict of interest All authors declare they have no conflict of interest.

Ethical approval This article does not contain any studies with human participants or animals performed by any authors.

References

Abbasi BA, Iqbal J, Mahmood T, Ahmad R, Kanwal S, Afridi S (2019) Plant-mediated synthesis of nickel oxide nanoparticles (NiO) via Geranium wallichianum: characterization and different biological applications. Mater Res Express 6:0850a7

Ahmed B, Solanki B, Zaidi A, Khan MS, Musarrat J (2019) Bacterial toxicity of biomimetic green zinc oxide nanoantibiotic: insights into ZnONP uptake and nanocolloid-bacteria interface. Toxicol Res (camb) 8:246–261

Amna T, Hassan MS, Yousef A, Mishra A, Barakat NAM, Khil MS, Kim HY (2013) Inactivation of foodborne pathogens by NiO/TiO2 Composite nanofibers: a novel biomaterial system. Food Bioprocess Technol 6:988–96

Angel Ezhilarasi A, Judith Vijaya J, Kaviyarasu K, John Kennedy L, Ramalingam RJ, Al-Lohedan HA (2018) Green synthesis of NiO nanoparticles using *Aegle marmelos* leaf extract for the evaluation of in-vitro cytotoxicity, antibacterial and photocatalytic properties. J Photochem Photobiol B Biol 180:39–50

Applerot G, Lellouche J, Lipovsky A, Nitzan Y, Lubart R, Gedanken A, Banin E (2012) Understanding the antibacterial mechanism

of CuO nanoparticles: revealing the route of induced oxidative stress. Small 8:3326–3337
Arakha M, Saleem M, Mallick BC, Jha S (2015) The effects of interfacial potential on antimicrobial propensity of ZnO nanoparticle. Sci Rep 5:1–10
Atri A, Echabaane M, Bouzidi A, Harabi I, Soucase BM, Ben Chaâbane R (2023) Green synthesis of copper oxide nanoparticles using Ephedra Alata plant extract and a study of their antifungal, antibacterial activity and photocatalytic performance under sunlight. Heliyon 9:1–16
Azizi-Lalabadi M, Ehsani A, Divband B, Alizadeh-Sani M (2019) Antimicrobial activity of Titanium dioxide and Zinc oxide nanoparticles supported in 4A zeolite and evaluation the morphological characteristic. Sci Rep 9:1–10
Behera N, Arakha M, Priyadarshinee M, Pattanayak BS, Soren S, Jha S, Mallick BC (2019) Oxidative stress generated at nickel oxide nanoparticle interface results in bacterial membrane damage leading to cell death. RSC Adv 9:24888–24894
Bepari S, Stevens-boyd R, Mohammad N, Li X, Abrokwah R, Kuila D (2020) Composite mesoporous SiO 2 -Al 2 O 3 supported Fe, FeCo and FeRu catalysts for Fischer-Tropsch studies in a 3-D printed stainless-steel microreactor materials today : proceedings composite mesoporous SiO 2 -Al 2 O 3 supported Fe, FeCo and FeRu catalysts. Mater Today Proc. https://doi.org/10.1016/j.matpr.2020.04.582
Davis R, Mauer L (2010) Fourier transform infrared (FT-IR) spectroscopy: a rapid tool for detection and analysis of foodborne pathogenic bacteria. Curr Res Technol Educ Top Appl Microbiol Microb Biotechnol A Méndez-Vilas 2:1582–94
Deng S, Zeng Z (2018) In vitro antibacterial activity and mechanism of monocaprylin against *Escherichia coli* and *Staphylococcus aureus*. J Food Prot 81:1988–1996
Devi KP, Nisha SA, Sakthivel R, Pandian SK (2010) Eugenol (an essential oil of clove) acts as an antibacterial agent against *Salmonella typhi* by disrupting the cellular membrane. J Ethnopharmacol 130:107–115
Ezhilarasi AA, Vijaya JJ, Kaviyarasu K, Maaza M, Ayeshamariam A, Kennedy LJ (2016) Green synthesis of NiO nanoparticles using Moringa oleifera extract and their biomedical applications: cytotoxicity effect of nanoparticles against HT-29 cancer cells. J Photochem Photobiol B Biol 164:352–360
Faghihzadeh F, Anaya NM, Schifman LA, Oyanedel-Craver V (2016) Fourier transform infrared spectroscopy to assess molecular-level changes in microorganisms exposed to nanoparticles. Nanotechnol Environ Eng 1:1–16
Giannousi K, Lafazanis K, Arvanitidis J, Pantazaki A, Dendrinousamara C (2014) Hydrothermal synthesis of copper based nanoparticles : antimicrobial screening and interaction with DNA. J Inorg Biochem 133:24–32
Guo N, Gai Q-Y, Jiao J, Wang W, Zu Y-G, Fu Y-J (2016) Antibacterial activity of fructus forsythia *Essential Oil* and the application of EO-loaded nanoparticles to food-borne pathogens. Foods 5:73
Halder S, Yadav KK, Sarkar R, Mukherjee S, Saha P, Haldar S, Karmakar S, Sen T (2015) Alteration of zeta potential and membrane permeability in bacteria: a study with cationic agents. Springerplus 4:1–14
Widiarti N, Sae JK, Wahyuni S (2017) Synthesis CuO-ZnO nanocomposite and its application as an antibacterial agent. IOP conference series: materials science and engineering, Vol 172, No. 1. IOP Publishing
Horie M, Nishio K, Fujita K, Kato H, Nakamura A, Kinugasa S, Endoh S, Miyauchi A, Yamamoto K, Murayama H, Niki E, Iwahashi H, Yoshida Y, Nakanishi J (2009) Ultrafine NiO particles induce cytotoxicity in vitro by cellular uptake and subsequent Ni(II) release. Chem Res Toxicol 22:1415–1426
Hou J, Wang X, Hayat T, Wang X (2017) Ecotoxicological effects and mechanism of CuO nanoparticles to individual organisms. Environ Pollut 221:209–217
Ismail NA, Shameli K, Wong MMT, Teow SY, Chew J, Sukri SNAM (2019) Antibacterial and cytotoxic effect of honey mediated copper nanoparticles synthesized using ultrasonic assistance. Mater Sci Eng C 104:109899
Jiang W, Saxena A, Song B, Ward BB, Beveridge TJ, Myneni SCB (2004) Elucidation of functional groups on gram-positive and gram-negative bacterial surfaces using infrared spectroscopy. Langmuir 20:11433–11442
Jin H, Huang X, Chen Y, Zhao H, Ye H, Huang F, Xing X, Cai J (2010) Photoinactivation effects of hematoporphyrin monomethyl ether on Gram-positive and-negative bacteria detected by atomic force microscopy. Appl Microbiol Biotechnol 88:761–770
John Owonubi S, Malima NM, Revaprasadu N (2020) Metal Oxide-Based Nanocomposites as Antimicrobial and Biomedical Agents. Elsevier Inc, The Netherlands
Jomova K, Baros S, Valko M (2012) Redox active metal-induced oxidative stress in biological systems. Transit Met Chem 37:127–134
Karthik K, Dhanuskodi S, Gobinath C, Prabukumar S, Sivaramakrishnan S (2018) Multifunctional properties of microwave assisted CdO–NiO–ZnO mixed metal oxide nanocomposite: enhanced photocatalytic and antibacterial activities. J Mater Sci Mater Electron 29:5459–5471
Khan I, Bahuguna A, Kumar P, Bajpai VK (2017) Antimicrobial potential of carvacrol against uropathogenic *Escherichia coli* via membrane disruption depolarization, and reactive oxygen species generation. Front Microbiol 8:1–9
Kiwi J, Nadtochenko V (2005) Evidence for the Mechanism of photocatalytic degradation of the bacterial wall membrane at the TiO 2 interface by ATR-FTIR and laser kinetic spectroscopy. Langmuir 21:4631–41
Ko JW, Kim SW, Hong J, Ryu J, Kang K, Park CB (2012) Synthesis of graphene-wrapped CuO hybrid materials by CO2 mineralization. Green Chem 14:2391–4
Kumar MP, Murugadoss G, Kumar MR (2020) Synthesis and characterization of CuO–NiO nanocomposite: highly active electrocatalyst for oxygen evolution reaction application. J Mater Sci Mater Electron 31:11286–11294
Kung ML, Tai MH, Lin PY, Wu DC, Wu WJ, Yeh BW, Hung HS, Kuo CH, Chen YW, Hsieh SL, Hsieh S (2017) Silver decorated copper oxide (Ag@CuO) nanocomposite enhances ROS-mediated bacterial architecture collapse. Colloids Surf B Biointerfaces 155:399–407
Lalithambika KC, Thayumanavan A, Ravichandran K, Sriram S (2017) Photocatalytic and antibacterial activities of eco-friendly green synthesized ZnO and NiO nanoparticles. J Mater Sci Mater Electron 28:2062–2068
Li H, Chen Q, Zhao J, Urmila K (2015) Enhancing the antimicrobial activity of natural extraction using the synthetic ultrasmall metal nanoparticles *Sci*. Rep 5:1–13
Mathelié-Guinlet M, Grauby-Heywang C, Martin A, Février H, Moroté F, Vilquin A, Béven L, Delville MH, Cohen-Bouhacina T (2018) Detrimental impact of silica nanoparticles on the nanomechanical properties of *Escherichia coli*, studied by AFM. J Colloid Interface Sci 529:53–64
Meghana S, Kabra P, Chakraborty S, Padmavathy N (2015) Understanding the pathway of antibacterial activity of copper oxide nanoparticles. RSC Adv 5:12293–12299
Mei L, Lu Z, Zhang W, Wu Z, Zhang X, Wang Y, Luo Y, Li C, Jia Y (2013) Bioconjugated nanoparticles for attachment and penetration into pathogenic bacteria. Biomaterials 34:10328–10337

Monga D, Basu S (2019) Enhanced photocatalytic degradation of industrial dye by g-C 3 N 4 /TiO 2 nanocomposite: role of shape of TiO 2 *Adv*. Powder Technol 30:1089–1098

Moniri Javadhesari S, Alipour S, Mohammadnejad S, Akbarpour MR (2019) Antibacterial activity of ultra-small copper oxide (II) nanoparticles synthesized by mechanochemical processing against *S. aureus* and *E. coli*. Mater Sci Eng C 105:110011

Morones JR, Elechiguerra JL, Camacho A, Holt K, Kouri JB, Ramírez JT, Yacaman MJ (2005) The bactericidal effect of silver nanoparticles. Nanotechnology 16:2346–2353

Naumann D (1984) Some ultrastructural information on intact, living bacterial cells and related cell-wall fragments as given by FTIR. Infrared Phys 24:233–8

Noman E, Al-Gheethi A, Talip BA, Mohamed R, Kassim AH (2019) Inactivating pathogenic bacteria in greywater by biosynthesized Cu/Zn nanoparticles from secondary metabolite of *Aspergillus iizukae* optimization, mechanism and techno economic analysis. PloS one 14:1–21

Patra JK, Das G, Baek K (2015) Antibacterial mechanism of the action of Enteromorpha linza L. essential oil against *Escherichia coli* and *Salmonella* typhimurium. Bot Stud. https://doi.org/10.1186/s40529-015-0093-7

Paul D, Neogi S (2019) Synthesis, characterization and a comparative antibacterial study of CuO, NiO and CuO–NiO mixed metal oxide. Mater Res Express 6:055004. https://doi.org/10.1088/2053-1591/ab003c

Paul D, Maiti S, Sethi DP, Neogi S (2020a) Bi-functional NiO-ZnO nanocomposite: synthesis, characterization, antibacterial and photo assisted degradation study. Adv Powder Technol. https://doi.org/10.1016/j.apt.2020.11.022

Paul D, Mangla S, Neogi S (2020b) Antibacterial study of CuO–NiO–ZnO trimetallic oxide nanoparticle. Mater Lett 271:127740. https://doi.org/10.1016/j.matlet.2020.127740

Qu Z, Liu P, Yang X, Wang F, Zhang W, Fei C (2016) Microstructure and characteristic of BiVO4 prepared under different pH values: photocatalytic efficiency and antibacterial activity. Materials (Basel) 9:129

Rahman MA, Radhakrishnan R, Gopalakrishnan R (2018) Structural, optical, magnetic and antibacterial properties of Nd doped NiO nanoparticles prepared by co-precipitation method. J Alloys Compd 742:421–429

Ramalingam B, Parandhaman T, Das SK (2016) Antibacterial effects of biosynthesized silver nanoparticles on surface ultrastructure and nanomechanical properties of gram-negative bacteria viz. *Escherichia coli* and *Pseudomonas aeruginosa*. ACS Appl Mater Interfaces 8:4963–4976

Sabouri Z, Akbari A, Hosseini HA, Hashemzadeh A, Darroudi M (2019) Eco-friendly biosynthesis of nickel oxide nanoparticles mediated by okra plant extract and investigation of their photocatalytic, magnetic, cytotoxicity, and antibacterial properties. J Clust Sci 30:1425–1434

Sahoo B, Sahu SK, Nayak S, Dhara D, Pramanik P (2012) Fabrication of magnetic mesoporous manganese ferrite nanocomposites as efficient catalyst for degradation of dye pollutants. Catal Sci Technol 2:1367–1374

Saito H, Sakakibara Y, Sakata A, Kurashige R, Murakami D, Kageshima H, Saito A, Miyazaki Y (2019) Antibacterial activity of lysozyme-chitosan oligosaccharide conjugates (LYZOX) against *Pseudomonas aeruginosa Acinetobacter Baumannii* and Methicillin-Resistant *Staphylococcus aureus*. PloS one 14:1–26

Sana S, Datta S, Biswas D, Sengupta D (2018) Assessment of synergistic antibacterial activity of combined biosurfactants revealed by bacterial cell envelop damage. Biochim Biophys Acta—Biomembr 1860:579–585

Siddiqi KS, ur Rahman A, Tajuddin N, Husen A (2018) Properties of zinc oxide nanoparticles and their activity against microbes. Nanoscale Res Lett. https://doi.org/10.1186/s11671-018-2532-3

Sirelkhatim A, Mahmud S, Seeni A (2015) Review on zinc oxide nanoparticles : antibacterial activity and toxicity mechanism. Nano-Micro Lett 7:219–242

Subhan MA, Ahmed T, Uddin N, Azad AK, Begum K (2015) Synthesis, characterization, PL properties, photocatalytic and antibacterial activities of nano multi-metal oxide NiO·CeO2·ZnO. Spectrochim. Acta—Part A Mol Biomol Spectrosc 136:824–831

Tripathi N, Goshisht MK (2022) Recent advances and mechanistic insights into antibacterial activity, antibiofilm activity, and cytotoxicity of silver nanoparticles. ACS Appl Bio Mater 5:1391–1463

Vaara M, Vaara T (1981) Outer membrane permeability barrier disruption by polymyxin in polymyxin-susceptible and -resistant Salmonella typhimurium. Antimicrob Agents Chemother 19:578–583

Vivek S, Preethi S, Sundramoorthy AK, Suresh Babu K (2020) The composition dependent structure and catalytic activity of nanostructured Cu-Ni bimetallic oxides. New J Chem 44:9691–9698

Wang Z, Lee YH, Wu B, Horst A, Kang Y, Tang YJ, Chen DR (2010) Anti-microbial activities of aerosolized transition metal oxide nanoparticles. Chemosphere 80:525–529

Wang H, Yi H, Chen X, Wang X (2013) Facile synthesis of a nanostructured nickel oxide electrode with outstanding pseudocapacitive properties. Electrochim Acta 105:353–361

Zhang L, Zhang L, Xu J (2020) Chemical composition, antibacterial activity and action mechanism of different extracts from hawthorn (*Crataegus pinnatifida* Bge.). Sci Rep 10:1–13